Dalton Transactions

ROYAL SOCIETY OF CHEMISTRY

PAPER

View Article Online
View Journal | View Issue

Cite this: *Dalton Trans.*, 2025, **54**, 6812

Regioselective oxidative bromination of arenes by a metal–organic framework-confined mono-bipyridyl iron(III) catalyst†

Rahul Kalita,‡[a] Aditya Kumar,‡[a] Poorvi Gupta,[a] Bharti Rana,[a] Bitan Sardar,[a] Manav Chauhan,[a] Biplab Ghosh,[b] Yukti Monga*[c] and Kuntal Manna *[a]

Oxidative bromination of arenes is an effective and environmentally friendly method for synthesizing bromoarenes. We have developed a highly robust zirconium metal–organic framework (MOF)-supported mono-bipyridyl iron(III) chloride catalyst (bpy-UiO-$FeCl_3$) for oxidative bromination of arenes using H_2O_2 as the oxidant and KBr as the bromine source. The bpy-UiO-$FeCl_3$ catalyst exhibits high conversion rates for various substituted arenes, yielding significant amounts of bromoarenes with excellent regioselectivity and recyclability under mild reaction conditions. The MOF catalyst outperforms its homogeneous counterparts in terms of both activity and regioselectivity due to the stabilization of the mononuclear bipyridyl-iron(III) species within the active sites within the MOF pores. Furthermore, the confinement of these active sites within the robust, well-defined, and uniform porous framework enhances the regioselectivity of bromination through shape-selective catalysis. The mechanism of bpy-UiO-$FeCl_3$-catalyzed oxidative bromination of arenes was thoroughly investigated by a combination of control experiments, spectroscopic analyses, and computational studies. These findings underscore the importance of MOFs in the development of heterogeneous catalysts based on Earth-abundant metals for the sustainable synthesis of haloarenes.

Received 22nd February 2025,
Accepted 24th March 2025

DOI: 10.1039/d5dt00443h

rsc.li/dalton

Introduction

Halogenation reactions have gained significant importance as organohalides are essential chemicals with significant efficacy in pharmaceutical sciences,[1] materials sciences,[2] imaging techniques,[3] and organic synthesis.[4–6] Bromoarenes, in particular, are important synthetic precursors for carbon–carbon bond formation reactions through Heck,[7] Stille,[8] and Suzuki[9] transmetallation processes. Furthermore, bromoaromatics serve as potent antibacterial, antifungal, and antiviral agents, as well as industrial intermediates in the production of pharmaceuticals, agrochemicals, and other specialty products.[10–20] Traditionally, bromination reactions are carried out using hazardous, toxic, and corrosive molecular bromine, often in combination with chlorinated solvents.[21,22] This approach poses significant environmental and health risks due to molecular bromine's toxicity and corrosive nature. Alternative methods involving electrophilic bromination using *N*-bromosuccinimide,[23,24] alkyl bromide/sodium hydride/DMSO combinations,[25] bromodimethylsulfonium bromide[26] and a hexamethylenetetramine bromine complex[27] have been explored.

Oxidative bromination has emerged as an attractive and environmentally benign alternative, as it generates electrophilic bromine using various oxidants.[28–34] This method offers a more sustainable and economically viable pathway to synthesize bromoaromatics compared to classical electrophilic substitutions. In particular, hydrogen peroxide is considered a promising oxidant for oxidative bromination, as the byproduct is only water. Most catalytic systems for oxidative bromination of arenes reported to date require acids,[35–39] which, while inexpensive and readily available, pose challenges related to product separation and hazardous waste generation.[40,41] Although oxidative bromination of arenes using bromide salts as halogen sources and oxidants has been explored,[34,42–45] there remains a pressing need for low-cost, Earth-abundant, non-toxic catalysts that enable oxidative bromination with high yields and excellent regioselectivity under mild conditions.

Metal–organic frameworks (MOFs) have attracted considerable interest for developing robust single-site heterogeneous Earth-abundant catalysts for various applications owing to

[a]*Department of Chemistry, Indian Institute of Technology Delhi, Hauz Khas, New Delhi 110016, India. E-mail: kmanna@chemistry.iitd.ac.in*
[b]*BARC Beamlines Section, Indus-2, RRCAT, Indore 452013, India*
[c]*Shyamlal College, Department of Chemistry, University of Delhi, Delhi, 110032, India. E-mail: yuktichem@shyamlal.du.ac.in*

†Electronic supplementary information (ESI) available. See DOI: https://doi.org/10.1039/d5dt00443h

‡These authors contributed equally.

their high porosity, crystallinity, and molecular tunability, enabling post-synthetic functionalization.[46–62] In particular, UiO-MOFs are unique due to the exceptional thermal and chemical stability provided by $Zr_6(\mu_3\text{-}O)_4(\mu_3\text{-}OH)_4$ secondary building units (SBUs) and linear dicarboxylate bridging linkers.[63–66] The post-synthetic modification of MOFs enables the functionalization of their organic linkers, facilitating the formation of single-site base-metal catalysts upon metalation. The rigid and porous MOF stabilizes coordinatively unsaturated and solution inaccessible base-metal species *via* active-site isolation by preventing multinuclear deactivation pathways.[67–75]

In addition, MOF-supported single-site catalysts combine the advantages of homogeneous catalysis, including uniform active site distribution, with the stability and recyclability of heterogeneous systems. Moreover, the confinement of active sites within the robust, well-defined and tunable porous frameworks increases the regioselectivity of the reaction *via* shape-selective catalysis.[76–81] Herein, we report the development of a highly active, selective and recyclable MOF-supported monomeric 2,2′-bipyridyl iron(III) chloride catalyst (bpy-UiO-$FeCl_3$) for oxidative bromination of arenes using H_2O_2 as the oxidant and KBr as the bromine source, affording bromoarenes with high yields and excellent regioselectivity under mild conditions (Fig. 1).

Results and discussion

Synthesis and characterization of bpy-UiO-$FeCl_3$

Bpy-UiO-$FeCl_3$ was synthesized through the post-synthetic metalation of the freshly prepared bpy-UiO-67 MOF containing bipyridyl-functionalized linkers (Fig. 1).[71,82] The synthesis involved a solvothermal reaction between $ZrCl_4$ and 2,2′-bipyridine-5,5′-dicarboxylic acid in the presence of CF_3CO_2H as a modulator in DMF at 100 °C for 4 days, affording the bpy-UiO-67 MOF with a 63% yield. The resulting pristine bpy-UiO-67 MOFs feature a three-dimensional porous UiO topology,[63] constructed from $Zr_6O_4(OH)_4$ nodes interconnected by 2,2′-bipyridine-5,5′-dicarboxylate (bpy) bridging linkers. By stirring a THF solution of $FeCl_3{\cdot}6H_2O$ with a slurry of bpy-UiO-67, we obtained bpy-UiO-$FeCl_3$, which contains bipyridyl-ligated Fe-trichloride species within its linkers. Analysis of digested bpy-UiO-$FeCl_3$ using Inductively Coupled Plasma-Optical Emission Spectroscopy (ICP-OES) revealed an Fe loading of approximately 45% with respect to the bipyridyl linker, which corresponds to the formula of $Zr_6(\mu_3\text{-}O)_4(\mu_3\text{-}OH)_4(bpy)_6Fe_{2.7}Cl_{8.1}$. The Powder X-Ray Diffraction (PXRD) pattern of bpy-UiO-$FeCl_3$ resembles that of the pristine bpy-UiO-67 MOF, indicating that the crystallinity and structure of the bpy-UiO-67 MOFs are retained during post-synthetic modification (Fig. 2a). Scanning Electron Microscopy-Energy Dispersive X-ray (SEM-EDX) analysis mapping of bpy-UiO-$FeCl_3$ demonstrated a uniform distribution of Fe and Zr ions within the MOF particles (Fig. 2b). Bpy-UiO-$FeCl_3$ has a Brunauer–Emmett–Teller (BET) surface area of 1235 $m^2\ g^{-1}$ and a pore size of 0.68 nm, which are smaller than those of the pristine bpy-UiO-67 MOF. This reduction in surface area and pore size is attributed to the incorporation of the iron moiety within the MOF pores (Fig. 2c). Thermogravimetric analysis (TGA) indicates that bpy-UiO-$FeCl_3$ is thermally stable up to 450 °C (Fig. S1, ESI†). X-ray Photoelectron Spectroscopy (XPS) analysis of bpy-UiO-$FeCl_3$ revealed the presence of Fe $2p_{3/2}$ and $2p_{1/2}$ binding energy peaks at 711.0 eV and 724.6 eV, respectively, confirming the +3 oxidation state of the iron ion (Fig. 2e). The +4 oxidation state of Zr ions in bpy-UiO-$FeCl_3$ was confirmed *via* XPS, which showed Zr^{4+} binding energies at 182.5 eV and 184.9 eV (Fig. S11, ESI†). In the X-ray Absorption Near Edge

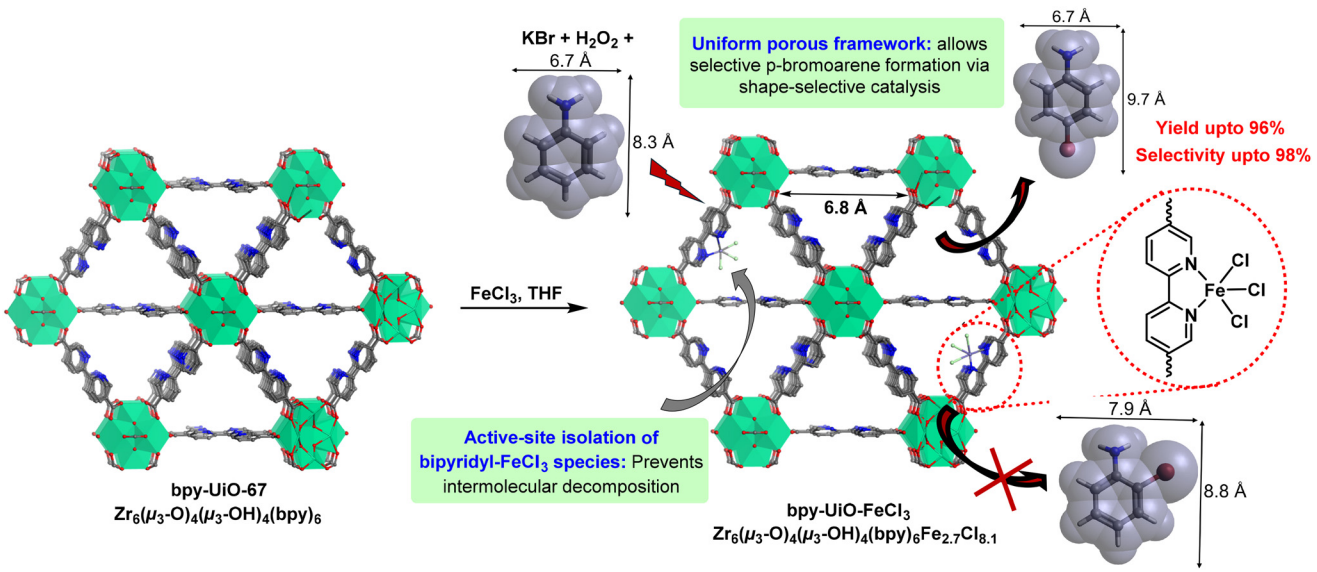

Fig. 1 Oxidative bromination of aniline using H_2O_2 and KBr with bpy-UiO-$FeCl_3$ as a shape-selective catalyst.

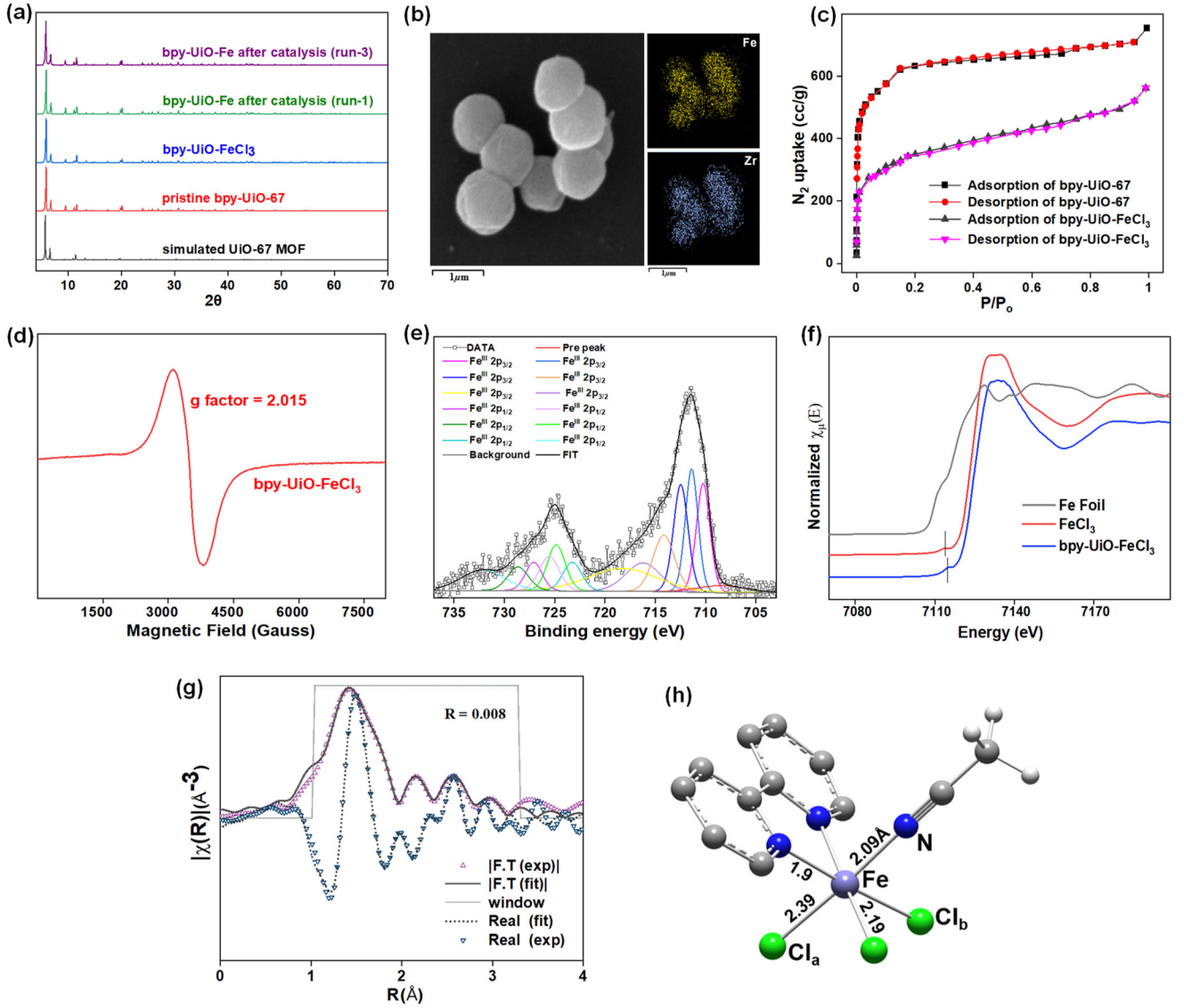

Fig. 2 (a) PXRD patterns of the simulated UiO-67 MOF (black), pristine bpy-UiO-67 (red), bpy-UiO-$FeCl_3$ (blue), bpy-UiO-Fe recovered after run-1 of oxidative bromination of aniline (green) and bpy-UiO-Fe recovered after run-3 of catalysis (purple). (b) SEM image of bpy-UiO-$FeCl_3$ particles along with elemental mapping of Fe and Zr. (c) N_2 sorption isotherms of bpy-UiO-67 (black/red)[83] and bpy-UiO-$FeCl_3$ (gray/magenta) measured at 77 K. (d) EPR spectrum of solid bpy-UiO-$FeCl_3$. (e) Fe 2p XPS spectrum of bpy-UiO-$FeCl_3$. (f) XANES spectra of metallic Fe(0) foil (gray), $FeCl_3$ (red) and bpy-UiO-$FeCl_3$ (blue). (g) EXAFS spectra and fits of bpy-UiO-$FeCl_3$ in the *R* space from 1.0 to 3.3 Å. (h) DFT-optimized structure of the bpy-$FeCl_3(NCCH_3)$ moiety within bpy-UiO-$FeCl_3$ MOFs. The bond distances are given in Å.

Structure (XANES) analysis, the pre-edge energy of Fe in bpy-UiO-$FeCl_3$ closely matched that of $FeCl_3$ at 7114 eV, further confirming the presence of Fe^{3+} species (Fig. 2f). The X-band electron paramagnetic resonance (EPR) spectrum reveals a broad signal centered at $g = 2.015$, indicating the presence of a high-spin Fe^{3+} species with low magnetic anisotropy (Fig. 2d).[84,85] Analysis of the Fe K-edge Extended X-ray Absorption Fine Structure (EXAFS) of bpy-UiO-$FeCl_3$ revealed that the Fe ion is octahedrally coordinated with two nitrogen atoms of bipyridine, three chloride ions, and one CH_3CN molecule (Fig. 2g). The Fe–$N_{bipyridine}$ distance is 1.9 Å, while the Fe–Cl_a distance is 2.39 Å, the Fe–Cl_b distance is 2.19 Å and the Fe–N_{CH_3CN} distance is 2.09 Å (Fig. 2h). The combined EXAFS and EPR data suggest the existence of a high-spin octahedral (bpy)$Fe^{III}(Cl)_3(NCCH_3)$ species within bpy-UiO-$FeCl_3$.

Catalytic oxidative bromination of aniline

Bpy-UiO-$FeCl_3$ is an active heterogeneous catalyst for the oxidative bromination of aniline, utilizing H_2O_2 as the oxidant and KBr as the brominating agent. To optimize the reaction conditions for maximum conversion and yield, we thoroughly investigated the impact of various reaction parameters, including the reaction temperature, reaction time, solvents, substrate-to-oxidant ratio, catalyst concentration, and nature and

concentration of the brominating agent. The effect of temperature on the oxidative bromination of aniline was studied over a range of 30–60 °C using 1 mmol of aniline, 4 mg of the catalyst bpy-UiO-$FeCl_3$ (0.4 mol% of Fe), 2 mmol of H_2O_2, 1.1 mmol of KBr, and 5 mL of CH_3CN for a duration of 2 h (Fig. 3a). The results showed that temperature variation had only a minimal effect on the conversion of aniline; however, regioselectivity decreased at higher temperatures (entries 1–3, Table S2, ESI†). The reaction time plays a critical role in evaluating the catalytic performance of the catalyst. To investigate this, the effect of reaction time on the oxidative bromination of aniline with H_2O_2 was examined over a range of 30–180 min (Fig. 3b). The results showed a direct correlation between the reaction time and the yield of the 4-bromoaniline product. The highest yield of 95% was achieved after 2 h, indicating that longer reaction times enhance substrate interaction and conversion, enabling the catalyst to effectively promote the desired reaction. The study revealed that CH_3CN was the most efficient solvent for the bpy-UiO-$FeCl_3$-catalyzed oxidative bromination of aniline using H_2O_2, achieving a conversion rate of 98% and a selectivity of 97% for the target product (**2a**) within 2 h (Fig. 3c). This enhanced performance is due to acetonitrile's beneficial solvation properties, which improve the stabilization of reaction intermediates and aid in the transfer of reactants at the catalyst's active sites.

In comparison, other solvents such as CH_3OH, DME and DCM resulted in lower yields of **2a**. A control experiment confirmed the necessity of H_2O_2, as no bromo product was produced in its absence (entry 8, Table S2, ESI†). An investigation of different H_2O_2 concentrations, while keeping other parameters constant, revealed that maximum bromination was achieved at a 1 : 2 molar ratio (Fig. 3d). In contrast, a 1 : 3 molar ratio resulted in a decreased yield (81%) and reduced *para*-selectivity (82%). The effect of different brominating agents on the oxidative bromination of aniline using H_2O_2 as the oxidant was also investigated (Fig. 3e). Among the

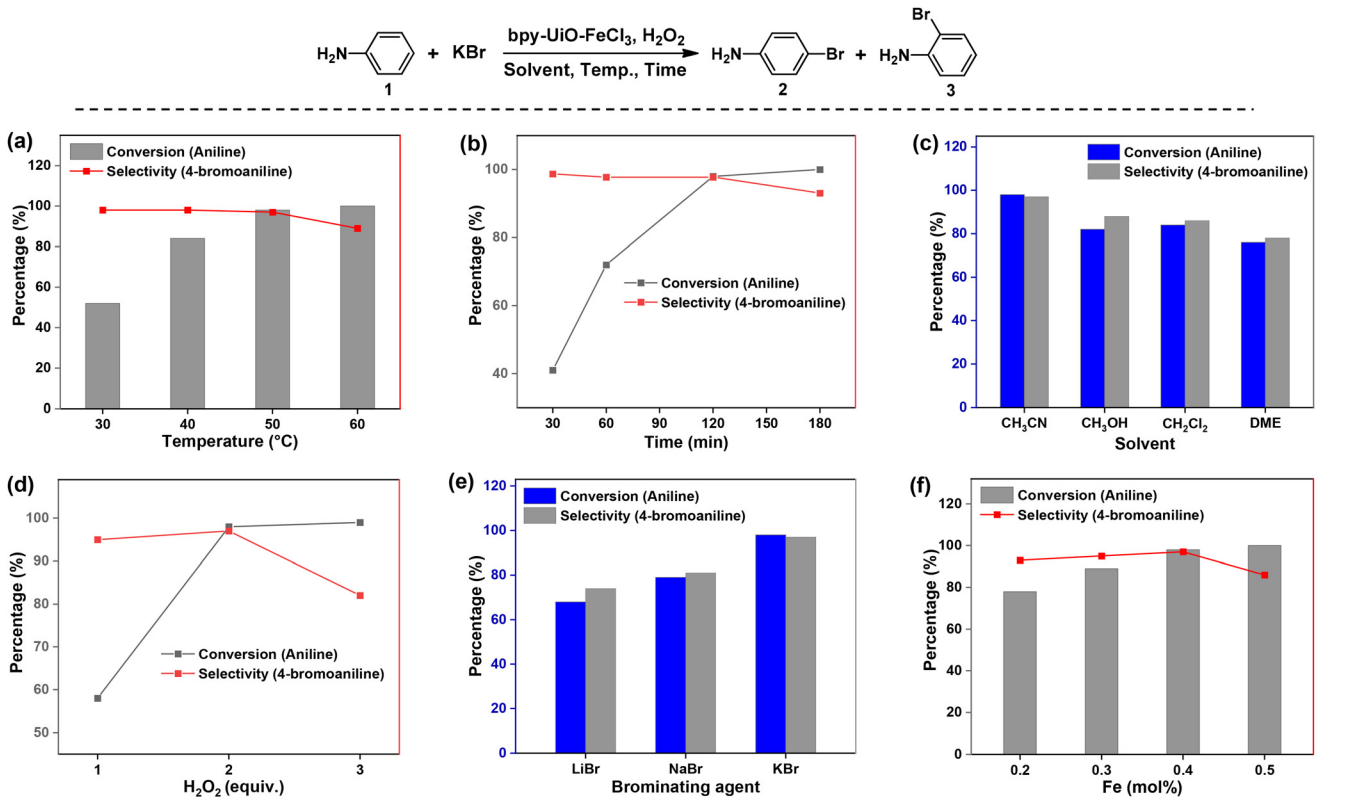

Fig. 3 (a) Effect of temperature on %conversion and %selectivity of 4-bromoaniline for bpy-UiO-$FeCl_3$-catalysed oxidative bromination of aniline. Reaction conditions: aniline (1 mmol), H_2O_2 (2 mmol), KBr (1.1 mmol), bpy-UiO-$FeCl_3$ (4 mg, 0.4 mol% of Fe), CH_3CN (5 mL), 2 h. (b) Effect of time on %conversion and %selectivity of 4-bromoaniline for bpy-UiO-$FeCl_3$-catalysed oxidative bromination of aniline. Reaction conditions: aniline (1 mmol), H_2O_2 (2 mmol), KBr (1.1 mmol), bpy-UiO-$FeCl_3$ (4 mg, 0.4 mol% of Fe), CH_3CN (5 mL), 50 °C. (c) Effect of different solvents on %conversion and %selectivity of 4-bromoaniline for bpy-UiO-$FeCl_3$-catalysed oxidative bromination of aniline. Reaction conditions: aniline (1 mmol), H_2O_2 (2 mmol), KBr (1.1 mmol), bpy-UiO-$FeCl_3$ (4 mg, 0.4 mol% of Fe), solvent (5 mL), 50 °C, 2 h. (d) Effect of H_2O_2 amounts on %conversion and %selectivity of 4-bromoaniline for bpy-UiO-$FeCl_3$-catalysed oxidative bromination of aniline. Reaction conditions: aniline (1 mmol), KBr (1.1 mmol), bpy-UiO-$FeCl_3$ (4 mg, 0.4 mol% of Fe), CH_3CN (5 mL), 50 °C, 2 h. (e) Effect of brominating agents on %conversion and %selectivity of 4-bromoaniline for bpy-UiO-$FeCl_3$-catalysed oxidative bromination of aniline. Reaction conditions: aniline (1 mmol), H_2O_2 (2 mmol), brominating agent (1.1 mmol), bpy-UiO-$FeCl_3$ (4 mg, 0.4 mol% of Fe), CH_3CN (5 mL), 50 °C, 2 h. (f) Effect of different Fe loadings on %conversion and %selectivity of 4-bromoaniline for bpy-UiO-$FeCl_3$-catalysed oxidative bromination of aniline. Reaction conditions: aniline (1 mmol), H_2O_2 (2 mmol), KBr (1.1 mmol), CH_3CN (5 mL), 50 °C, 2 h.

brominating agents tested (LiBr, NaBr, and KBr), KBr demonstrated the highest efficiency, achieving 98% conversion with excellent regioselectivity for the *para*-product (97%). In comparison, NaBr and LiBr showed lower activities (entries 11 and 12, Table S2, ESI†). A KBr concentration of 1.1 mmol yielded the optimal results. The catalyst loading was systematically optimized to achieve maximum efficiency. It was observed that 0.4 mol% of Fe loading in bpy-UiO-$FeCl_3$ provided the highest conversion rate of 98%. Reducing the Fe loading in the bpy-UiO-$FeCl_3$ catalyst from 0.4 mol% to 0.2 mol% resulted in a decline in bromoaniline yield from 95% to 73%, attributed to a reduced availability of active sites. Under the optimized conditions, the reaction achieved the highest yield of 4-bromoaniline (**2a**) at 95%. This was accomplished using a catalyst loading of 0.4 mol% Fe, 1 mmol of aniline, 1.1 mmol of KBr, and 2 mmol of 30% aqueous H_2O_2 in 5 mL of CH_3CN at 50 °C for 2 hours, resulting in a turn-over number (TON) of 238 (entry 2, Table S2, ESI†).

Substrate scopes for oxidative bromination of arenes

Under the optimized conditions, the oxidative bromination of aromatic substrates, including *N*,*N*-dimethylaniline (**1b**), anisole (**1c**), phenol (**1d**), and toluene (**1e**), afforded the corresponding *para*-bromo products (**2b–2e**) with isolated yields ranging from 85% to 96% and excellent selectivity (91–98%). Benzene (**1f**), due to its lack of activating groups, exhibited significantly lower conversion rates and required extended reaction times to achieve measurable bromination under the same conditions. In contrast, deactivated aromatic rings such as nitrobenzene (**1g**) and bromobenzene (**1h**) produced the corresponding bromo products with yields of 15–20% after 24 h at 80 °C. 4-Substituted aromatics, such as 4-methylaniline (**1i**) and *p*-xylene (**1j**), were selectively converted to 2-bromo-4-methylaniline (**2i**) and 2-bromo-*p*-xylene (**2j**) with isolated yields of 70–71%. In contrast, 2-substituted aromatics such as *o*-xylene (**1k**), 2-iodoaniline (**1l**), 1,2-dimethoxybenzene (**1m**) and catechol (**1n**) were also selectively converted to the corresponding bromo products (**2k–n**) with isolated yields of 57–72%. Similarly, 3-substituted aromatics such as 3-methylaniline (**1o**) and *m*-xylene (**1p**) were selectively converted to 4-bromo-3-methylaniline (**2o**) and 4-bromo-*m*-xylene (**2p**), respectively, achieving yields of 66–67% under the same conditions (Scheme 1).

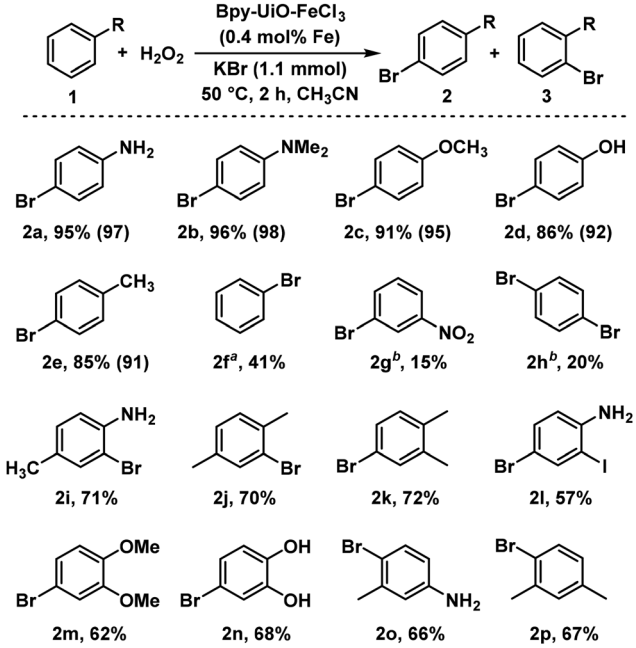

Scheme 1 Substrate scope of oxidative bromination of arenes with bpy-UiO-$FeCl_3$. Conditions: **1** (1 mmol), H_2O_2 (2 mmol), KBr (1.1 mmol), bpy-UiO-$FeCl_3$ (4 mg, 0.4 mol% of Fe), CH_3CN (5 mL), 50 °C, 2 h. Yields refer to the isolated products. Selectivity of *para*-bromo products is given in parentheses. [a]The reaction was performed for 10 h. [b]The reaction was performed for 24 h at 80 °C.

Control experiments

Bpy-UiO-$FeCl_3$ acts as a heterogeneous catalyst and can be recycled at least three times while maintaining consistent activity (Fig. 4a). The PXRD pattern of the recovered MOF material after catalysis revealed no apparent change in crystallinity and structure of the MOFs (Fig. 2a). The percentage of leached Fe and Zr into the supernatant after the first run was 0.02% and 0.6%, respectively, while after the third run, it was 0.08% and 1.5%, as analyzed by ICP-OES (Table S5, ESI†). The catalytic activity of bpy-UiO-$FeCl_3$ is over four times greater than that of the homogeneous control, bipyridine-$FeCl_3$. The latter was synthesized by reacting 5,5′-dimethyl-2,2′-bipyridine with $FeCl_3{\cdot}6H_2O$ in a 1 : 1 molar ratio in THF. The time evolution plot for bpy-UiO-$FeCl_3$ (0.4 mol% of Fe) catalyzed oxidative bromination of aniline demonstrates a linear increase in the synthesis of 4-bromoaniline, achieving 97% selectivity until 98% conversion of aniline in 2 h (Fig. 4b). In contrast, under the same reaction conditions and with equivalent Fe loading, bipyridine-$FeCl_3$ produced only 26% yield of 4-bromoaniline in 2 hours, with a selectivity of 68% (Fig. 4b). This enhanced activity of the bpy-UiO-$FeCl_3$ MOF is attributed to the stability of bpy-$FeCl_3$ species, which are isolated at the linkers, preventing decomposition.

In addition, the bpy-UiO-$FeCl_3$ framework features uniform and rigid pores with a size of 0.68 nm, which allow the diffusion of aniline (0.83 × 0.67 nm) and *p*-bromoaniline (0.97 × 0.67 nm); however, they restrict the formation of the larger product, *o*-bromoaniline (0.88 × 0.79 nm), resulting in the formation of *p*-bromoaniline with 97% selectivity through shape-selective catalysis. While the MOF pores (0.68 nm) are indeed identical to or smaller than the reported molecular widths of aniline (0.83 × 0.67 nm) and *para*-bromoaniline products (0.97 × 0.67 nm), molecules are not rigid and can reorient or deform during diffusion and enter the pore by aligning its narrower axis (0.67 nm) with the pore window.[76] In contrast, the homogeneous bipyridine-$FeCl_3$ catalyst lacks this structural confinement, leading to only 68% selectivity of *p*-bromoaniline. To confirm that the oxidative bromination reaction occurs predominantly within the pores of the bpy-UiO-$FeCl_3$ MOF, rather

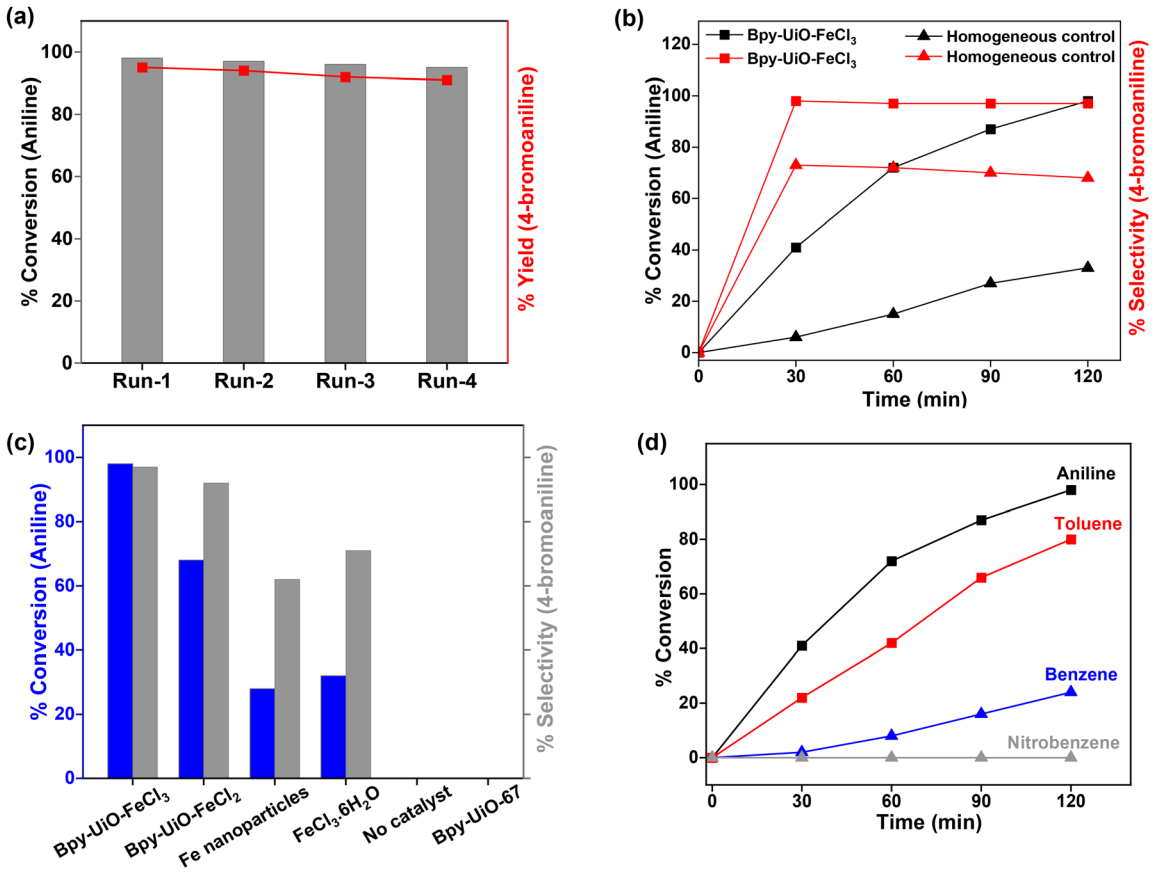

Fig. 4 (a) Plot for the %conversion of aniline and the %yield of 4-bromoaniline at various runs in the recycling of bpy-UiO-$FeCl_3$-catalyzed oxidative bromination of aniline. (b) Time evaluation studies of oxidative bromination of aniline using bpy-UiO-$FeCl_3$ and its homogeneous control [(bpy)$FeCl_3$] under identical conditions. Conditions: aniline (1 mmol), H_2O_2 (2 mmol), KBr (1.1 mmol), catalyst (0.4 mol% of Fe), CH_3CN (5 mL), 50 °C. (c) Comparison of the catalytic activity of bpy-UiO-$FeCl_3$ with other iron catalysts under identical reaction conditions. Conditions: aniline (1 mmol), H_2O_2 (2 mmol), KBr (1.1 mmol), catalyst (0.4 mol% of Fe), CH_3CN (5 mL), 50 °C, 2 h. (d) Time evaluation studies of oxidative bromination of aniline, toluene, benzene and nitrobenzene under the optimized reaction conditions.

than on the external surface of the MOF, an experiment was conducted using a bulky phosphine, tricyclohexylphosphine, to block the surface iron active sites.[74,76] The addition of 1.2 equivalents of tricyclohexylphosphine per iron ion in the bpy-UiO-$FeCl_3$-catalysed oxidative bromination of aniline resulted in a slight decrease in conversion to ~88%. However, the regioselectivity for the *para*-bromoaniline product remained unchanged (97%). This observation suggests that the iron active sites are mostly embedded within the MOF pores, which catalyze the oxidative bromination of arenes within the pores (entry 8, Table S3, ESI†). Several controlled experiments were conducted to identify the actual catalytic species involved in the bpy-UiO-$FeCl_3$-catalyzed oxidative bromination of aniline to produce 4-bromoaniline. The results showed that reactions (a) without the bpy-UiO-$FeCl_3$ catalyst (entry 3, Table S3†) and (b) with the pristine bpy-UiO-67 MOF (entry 2, Table S3†) all yielded negligible amounts of 4-bromoaniline. The results also showed that reactions (a) with bpy-UiO-$FeCl_2$ (entry 4, Table S2†), (d) with $FeCl_3{\cdot}6H_2O$ (entry 5, Table S2†) and (e) with Fe nanoparticles (entry 6, Table S2†) all yielded lower amounts of 4-bromoaniline with less selectivity (Fig. 4c). This confirms that bpy-UiO-$FeCl_3$ is the active catalyst for the oxidative bromination of aniline. The oxidative bromination of aniline ceased upon the removal of the solid MOF catalyst, indicating that the active species is embedded in the MOF solid (section 3.4, ESI†).

Mechanism exploration of bpy-UiO-$FeCl_3$-catalyzed oxidative bromination of aniline

The mechanism of bpy-UiO-$FeCl_3$-catalyzed oxidative bromination of aniline was investigated by characterizing the catalyst after catalysis and computational studies. The PXRD pattern of the recovered bpy-UiO-Fe MOF after catalysis indicates that both the structure and crystallinity of the MOF remained intact during the reaction (Fig. 2a). Additionally, the absence of any characteristic peak for metallic iron at higher 2θ angles in the same PXRD pattern suggests that Fe(0) nanoparticles or metallic Fe particulates did not form during the bromination reaction. The XPS analysis of bpy-UiO-$FeCl_3$ after oxidative bromination of aniline identified Fe $2p_{3/2}$ and $2p_{1/2}$ binding energy peaks at 711.8 eV and 724.6 eV, respectively, confirming the +3 oxidation state of the iron ion (Fig. S12, ESI†). Again,

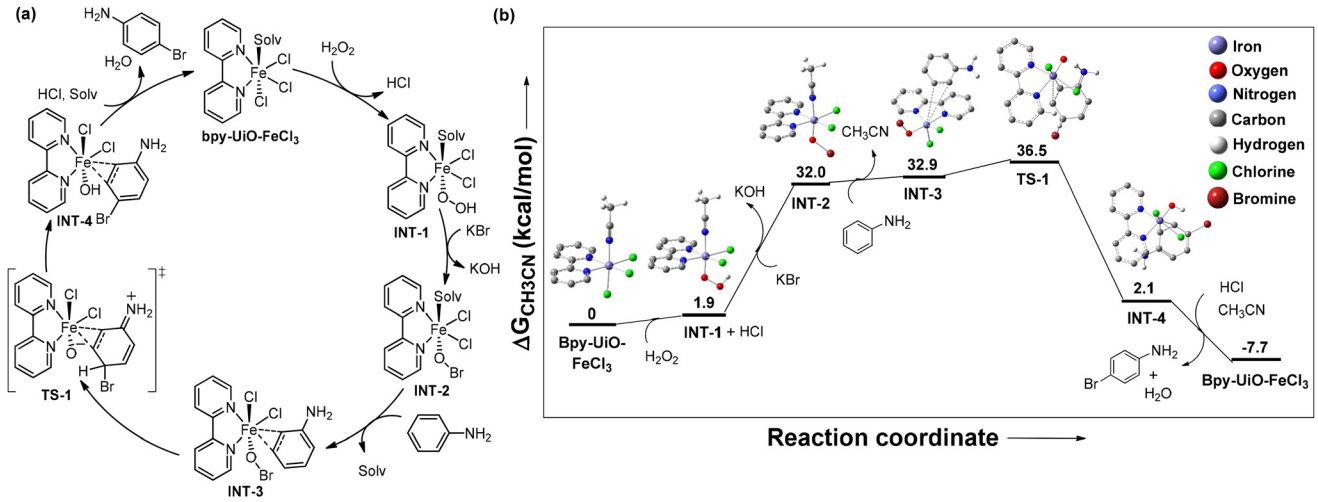

Fig. 5 (a) Proposed catalytic cycle of bpy-UiO-$FeCl_3$-catalyzed oxidative bromination of arenes. (b) DFT-calculated free energy profile diagram of bpy-UiO-$FeCl_3$-catalyzed oxidative bromination of aniline at 323.15 K.

radical pathway tests utilizing Na_2SO_3 and *tert*-butanol (TBA) as scavengers demonstrated no impact on the reaction rate, effectively ruling out the possibility of a radical mechanism (Fig. S6, ESI†).

Based on spectroscopic data and control experiments, we propose that the reaction of H_2O_2 with bpy-UiO-$FeCl_3$ initially forms an Fe(III)-hydroperoxy intermediate, [Fe^{III}-OOH] (INT-1). Subsequently, the Br^- ion from KBr attacks the oxygen atom coordinated to iron in INT-1, forming the [Fe^{III}-OBr] intermediate (INT-2) and releasing KOH. INT-2 interacts with the aniline substrate to form INT-3, where electrophilic aromatic substitution takes place. The reactive Br^+ then undergoes an electrophilic attack on the aniline substrate, resulting in the formation of the bromoaniline-bound Fe(III) intermediate (INT-4) *via* transition state 1 (TS-1). Finally, the desired *p*-bromoaniline product is released from INT-4, regenerating the initial Fe(III) catalyst, bpy-UiO-Fe, and completing the catalytic cycle (Fig. 5a).

Evidence for the electrophilic aromatic substitution mechanism was gathered through a time-evolution study of reactions involving arenes such as aniline, toluene, benzene, and nitrobenzene under identical conditions (Fig. 4d). The reaction rates followed the trend aniline > toluene > benzene, consistent with the activating effects of electron-donating groups. In contrast, nitrobenzene did not undergo the reaction due to the deactivating influence of its electron-withdrawing nitro group, rendering the aromatic system unreactive under these conditions.

To gain a deeper understanding of the reaction pathway, we computed the entire catalytic cycle using Density Functional Theory (DFT) at the B3LYP/def2-SVP/SMD (solvent = acetonitrile) level of theory in Gaussian 09 software (Fig. 5b). The DFT-calculated free energy diagram at 323.15 K for the bpy-UiO-$FeCl_3$-catalyzed oxidative bromination of aniline indicates that the coordination of H_2O_2 with the bpy-UiO-$FeCl_3$ MOF is endergonic by 1.9 kcal mol^{-1}. Furthermore, nucleophilic substitution of Br^- on [Fe^{III}(OOH)] leading to the formation of [Fe^{III}(OBr)] species (INT-2) is endergonic by 30.1 kcal mol^{-1}. In the next step, the conversion of INT-2 to INT-3 is endergonic by 0.9 kcal mol^{-1}. The subsequent transformation of INT-3 to INT-4 *via* TS-1 is exergonic by 34.4 kcal mol^{-1}, overcoming a barrier of 3.6 kcal mol^{-1}. Finally, the release of *p*-bromoaniline from INT-4 regenerates the bpy-UiO-Fe MOF, which is exergonic by 9.8 kcal mol^{-1}. DFT calculations suggest that the nucleophilic substitution of Br^- on INT-1 leading to the formation of INT-2 is the turnover limiting step requiring a free activation energy of 30.1 kcal mol^{-1} (Fig. 5b).

Conclusions

In summary, we have successfully synthesized a porous and highly robust zirconium-based metal–organic framework (MOF)-supported mono-bipyridyl-iron(III) chloride catalyst through active-site isolation. Bpy-UiO-$FeCl_3$ demonstrates high selectivity and recyclability for the oxidative bromination of various substituted arenes using hydrogen peroxide (H_2O_2) as the oxidant and potassium bromide (KBr) as the bromine source. Mono-substituted arenes were converted to *para*-bromoarenes with excellent selectivities ranging from 90% to 98%. The uniform and regular porous structure of the MOF facilitates shape-selective catalysis, preventing the formation of larger *ortho*-bromoarene products, ensuring the exclusive formation of *para*-bromoarenes, unlike homogeneous catalysts that typically exhibit lower selectivity. Bpy-UiO-$FeCl_3$ is also effective for a wide range of 1,2-, 1,3-, and 1,4-substituted arenes, converting them into the desired bromo products with moderate to good yields under mild reaction conditions. Through spectroscopic and computational studies, we investigated the mechanism and identified the turnover-limiting step

in the catalytic cycle. Our findings highlight the importance of MOFs in creating sustainable, Earth-abundant metal catalysts for the direct oxidative bromination of arenes, enabling the eco-friendly synthesis of haloarenes.

Author contributions

R. K. and A. K. synthesized the MOF catalyst and performed catalytic reactions. P. G. performed the DFT calculations. R. K., B. R., B. S. and M. C. characterized the MOF materials and analyzed the data. K. M. designed and supervised the entire project. K. M. and R. K. wrote the manuscript. All the authors approved the final version of the manuscript.

Data availability

The data supporting this article have been included as part of the ESI.†

Conflicts of interest

There are no conflicts to declare.

Acknowledgements

K. M. thanks the Science and Engineering Research Board (SERB), India [CRG/2022/003553] and CSIR-HRDG [01(3040)/21/EMR-II] for financial support. R. K., P. G., B. R. and M. C. acknowledge the CSIR. A. K. acknowledges the UGC for financial support. B. S. acknowledges ANRF NPDF (PDF/2023/000250) for financial support. The authors thank Prof. B. Jayaram for providing access to his super-computing facility. We acknowledge Raja Ramanna Centre for Advanced Technology-Indore (RRCAT) for XAS measurement in the Indus-2 SRS facility. We thank Rajashri Urkude for her help in XAS measurement at RRCAT. The authors acknowledge the Central Research Facility, IIT Delhi, for XPS, NMR, BET, SEM, EPR and other instrument facilities.

References

1 M. Hernandes, S. M. Cavalcanti, D. R. Moreira, W. De Azevedo Junior and A. C. Leite, *Curr. Drug Targets*, 2010, **11**, 303–314.
2 M. L. Tang and Z. Bao, *Chem. Mater.*, 2011, **23**, 446–455.
3 M. J. Adam and D. S. Wilbur, *Chem. Soc. Rev.*, 2005, **34**, 153.
4 D. A. Petrone, J. Ye and M. Lautens, *Chem. Rev.*, 2016, **116**, 8003–8104.
5 P. A. Champagne, J. Desroches, J.-D. Hamel, M. Vandamme and J.-F. Paquin, *Chem. Rev.*, 2015, **115**, 9073–9174.
6 A. Varenikov, E. Shapiro and M. Gandelman, *Chem. Rev.*, 2021, **121**, 412–484.
7 R. F. Heck, in *Organic Reactions*, ed. S. E. Denmark, Wiley, 1st edn, 1982, pp. 345–390.
8 J. K. Stille, *Angew. Chem., Int. Ed. Engl.*, 1986, **25**, 508–524.
9 A. Suzuki, *Angew. Chem., Int. Ed.*, 2011, **50**, 6722–6737.
10 D. Wischang, O. Brücher and J. Hartung, *Coord. Chem. Rev.*, 2011, **255**, 2204–2217.
11 I. Saikia, A. J. Borah and P. Phukan, *Chem. Rev.*, 2016, **116**, 6837–7042.
12 M. Naresh, M. Arun Kumar, M. Mahender Reddy, P. Swamy, J. Nanubolu and N. Narender, *Synthesis*, 2013, **45**, 1497–1504.
13 N. Oztaskin, S. Goksu, Y. Demir, A. Maras and İ. Gulcin, *Molecules*, 2022, **27**, 7426.
14 Y. Yoshida, T. Mino and M. Sakamoto, *ACS Catal.*, 2021, **11**, 13028–13033.
15 G. W. Gribble, *Acc. Chem. Res.*, 1998, **31**, 141–152.
16 M. J. Dagani, H. J. Barda, T. J. Benya and D. C. Sanders, in *Ullmann's Encyclopedia of Industrial Chemistry*, ed. Wiley-VCH, Wiley, 1st edn, 2000.
17 P. Ruiz-Castillo and S. L. Buchwald, *Chem. Rev.*, 2016, **116**, 12564–12649.
18 N. Longkumer, K. Richa, R. Karmaker, V. Kuotsu, A. Supong, L. Jamir, P. Bharali and U. B. Sinha, *Acta Chim. Slov.*, 2019, **66**, 276–283.
19 N. Miyaura and A. Suzuki, *Chem. Rev.*, 1995, **95**, 2457–2483.
20 A. Jain, L. S. Duvvuri, S. Farah, N. Beyth, A. J. Domb and W. Khan, *Adv. Healthcare Mater.*, 2014, **3**, 1969–1985.
21 R. Adams and C. S. Marvel, *Org. Synth.*, 1921, **1**, 39.
22 C. Venkatachalapathy and K. Pitchumani, *Tetrahedron*, 1997, **53**, 2581–2584.
23 B. Das, K. Venkateswarlu, M. Krishnaiah and H. Holla, *Tetrahedron Lett.*, 2006, **47**, 8693–8697.
24 D. A. Rogers, R. G. Brown, Z. C. Brandeburg, E. Y. Ko, M. D. Hopkins, G. LeBlanc and A. A. Lamar, *ACS Omega*, 2018, **3**, 12868–12877.
25 M. Guo, L. Varady, D. Fokas, C. Baldino and L. Yu, *Tetrahedron Lett.*, 2006, **47**, 3889–3892.
26 G. Majetich, R. Hicks and S. Reister, *J. Org. Chem.*, 1997, **62**, 4321–4326.
27 M. M. Heravi, N. Abdolhosseini and H. A. Oskooie, *Tetrahedron Lett.*, 2005, **46**, 8959–8963.
28 B. Sels, D. D. Vos, M. Buntinx, F. Pierard, A. Kirsch-De Mesmaeker and P. Jacobs, *Nature*, 1999, **400**, 855–857.
29 B. M. Choudary, Y. Sudha and P. N. Reddy, *Synlett*, 1994, 450–450.
30 G. Rothenberg and J. H. Clark, *Org. Process Res. Dev.*, 2000, **4**, 270–274.
31 N. Narender, P. Srinivasu, S. J. Kulkarni and K. V. Raghavan, *Synth. Commun.*, 2000, **30**, 3669–3675.
32 B. Ganchegui and W. Leitner, *Green Chem.*, 2007, **9**, 26–29.
33 A. Podgoršek, M. Zupan and J. Iskra, *Angew. Chem., Int. Ed.*, 2009, **48**, 8424–8450.
34 D.-B. Jiang, F.-Y. Wu and H.-L. Cui, *Org. Biomol. Chem.*, 2023, **21**, 1571–1590.

35 S. Mallik, K. M. Parida and S. S. Dash, *J. Mol. Catal. A: Chem.*, 2007, **261**, 172–179.
36 T. Moriuchi, Y. Fukui, T. Sakuramoto and T. Hirao, *Chem. Lett.*, 2017, **46**, 1708–1710.
37 M. R. Maurya, V. Prakash, F. Avecilla and M. Sankar, *Eur. J. Inorg. Chem.*, 2021, **2021**, 1685–1694.
38 H. H. L. B. Lima, G. R. da Silva, J. M. Pena and R. Cella, *ChemistrySelect*, 2017, **2**, 9624–9627.
39 E. M. Gayakwad, K. P. Patel and G. S. Shankarling, *New J. Chem.*, 2019, **43**, 6001–6009.
40 T. Okuhara, *Chem. Rev.*, 2002, **102**, 3641–3666.
41 K. Wilson and J. H. Clark, *Pure Appl. Chem.*, 2000, **72**, 1313–1319.
42 S. Eshwar Rao and G. Virupaiah, *J. Chem. Technol. Biotechnol.*, 2017, **92**, 2060–2074.
43 E. E. Alberto, L. M. Muller and M. R. Detty, *Organometallics*, 2014, **33**, 5571–5581.
44 G. Zhao, E. Wang and R. Tong, *ACS Sustainable Chem. Eng.*, 2021, **9**, 6118–6125.
45 G. Pomarico, F. Sabuzi, V. Conte and P. Galloni, *New J. Chem.*, 2019, **43**, 17774–17782.
46 T. Ikuno, J. Zheng, A. Vjunov, M. Sanchez-Sanchez, M. A. Ortuño, D. R. Pahls, J. L. Fulton, D. M. Camaioni, Z. Li, D. Ray, B. L. Mehdi, N. D. Browning, O. K. Farha, J. T. Hupp, C. J. Cramer, L. Gagliardi and J. A. Lercher, *J. Am. Chem. Soc.*, 2017, **139**, 10294–10301.
47 S. M. Cohen, *Chem. Rev.*, 2012, **112**, 970–1000.
48 Z. Lin, N. C. Thacker, T. Sawano, T. Drake, P. Ji, G. Lan, L. Cao, S. Liu, C. Wang and W. Lin, *Chem. Sci.*, 2018, **9**, 143–151.
49 N. C. Thacker, Z. Lin, T. Zhang, J. C. Gilhula, C. W. Abney and W. Lin, *J. Am. Chem. Soc.*, 2016, **138**, 3501–3509.
50 D. Y. Osadchii, A. I. Olivos-Suarez, Á. Szécsényi, G. Li, M. A. Nasalevich, I. A. Dugulan, P. S. Crespo, E. J. M. Hensen, S. L. Veber, M. V. Fedin, G. Sankar, E. A. Pidko and J. Gascon, *ACS Catal.*, 2018, **8**, 5542–5548.
51 J. N. Hall and P. Bollini, *Chem. – Eur. J.*, 2020, **26**, 16639–16643.
52 Y. Yang, S. Kanchanakungwankul, S. Bhaumik, Q. Ma, S. Ahn, D. G. Truhlar and J. T. Hupp, *J. Am. Chem. Soc.*, 2023, **145**, 22019–22030.
53 M. C. Simons, S. D. Prinslow, M. Babucci, A. S. Hoffman, J. Hong, J. G. Vitillo, S. R. Bare, B. C. Gates, C. C. Lu, L. Gagliardi and A. Bhan, *J. Am. Chem. Soc.*, 2021, **143**, 12165–12174.
54 Y. Zhang, J. Li, X. Yang, P. Zhang, J. Pang, B. Li and H.-C. Zhou, *Chem. Commun.*, 2019, **55**, 2023–2026.
55 B. Pramanik, R. Sahoo and M. C. Das, *Coord. Chem. Rev.*, 2023, **493**, 215301.
56 P. Gupta, B. Rana, R. Maurya, R. Kalita, M. Chauhan and K. Manna, *Chem. Sci.*, 2025, **16**, 2785–2795.
57 M. Chauhan, B. Rana, P. Gupta, R. Kalita, C. Thadhani and K. Manna, *Nat. Commun.*, 2024, **15**, 9798.
58 W. Begum, M. Chauhan, R. Kalita, P. Gupta, N. Akhtar, N. Antil, R. Newar and K. Manna, *ACS Catal.*, 2024, **14**, 10427–10436.
59 R. Newar, W. Begum, N. Akhtar, N. Antil, M. Chauhan, A. Kumar, P. Gupta, J. Malik, Balendra and K. Manna, *Eur. J. Inorg. Chem.*, 2022, **2022**, e202101019.
60 R. Newar, R. Kalita, N. Akhtar, N. Antil, M. Chauhan and K. Manna, *Catal. Sci. Technol.*, 2022, **12**, 6795–6804.
61 N. Antil, A. Kumar, N. Akhtar, R. Newar, W. Begum and K. Manna, *Inorg. Chem.*, 2021, **60**, 9029–9039.
62 R. Kalita, W. Begum, P. Gupta, M. Chauhan, N. Akhtar, R. Newar and K. Manna, *Eur. J. Inorg. Chem.*, 2023, **26**, e202300215.
63 J. H. Cavka, S. Jakobsen, U. Olsbye, N. Guillou, C. Lamberti, S. Bordiga and K. P. Lillerud, *J. Am. Chem. Soc.*, 2008, **130**, 13850–13851.
64 Y. Bai, Y. Dou, L.-H. Xie, W. Rutledge, J.-R. Li and H.-C. Zhou, *Chem. Soc. Rev.*, 2016, **45**, 2327–2367.
65 A. Das, N. Anbu, M. Sk, A. Dhakshinamoorthy and S. Biswas, *Eur. J. Inorg. Chem.*, 2020, **2020**, 2830–2834.
66 S. Yuan, J.-S. Qin, C. T. Lollar and H.-C. Zhou, *ACS Cent. Sci.*, 2018, **4**, 440–450.
67 J. Baek, B. Rungtaweevoranit, X. Pei, M. Park, S. C. Fakra, Y.-S. Liu, R. Matheu, S. A. Alshmimri, S. Alshehri, C. A. Trickett, G. A. Somorjai and O. M. Yaghi, *J. Am. Chem. Soc.*, 2018, **140**, 18208–18216.
68 J. Lee, O. K. Farha, J. Roberts, K. A. Scheidt, S. T. Nguyen and J. T. Hupp, *Chem. Soc. Rev.*, 2009, **38**, 1450.
69 K. Manna, T. Zhang and W. Lin, *J. Am. Chem. Soc.*, 2014, **136**, 6566–6569.
70 Y.-S. Wei, M. Zhang, R. Zou and Q. Xu, *Chem. Rev.*, 2020, **120**, 12089–12174.
71 T. Zhang, K. Manna and W. Lin, *J. Am. Chem. Soc.*, 2016, **138**, 3241–3249.
72 C. Kutzscher, G. Nickerl, I. Senkovska, V. Bon and S. Kaskel, *Chem. Mater.*, 2016, **28**, 2573–2580.
73 N. Akhtar, M. Chauhan, P. Gupta, N. Antil and K. Manna, *Dalton Trans.*, 2023, **52**, 15384–15393.
74 R. Kalita, M. Chauhan, P. Gupta, W. Begum and K. Manna, *Angew. Chem.*, 2025, **64**, e202413402.
75 P. Gupta, N. Akhtar, W. Begum, B. Rana, R. Kalita, M. Chauhan, C. Thadhani and K. Manna, *Inorg. Chem.*, 2024, **63**, 11907–11916.
76 X. Zhang, Z. Huang, M. Ferrandon, D. Yang, L. Robison, P. Li, T. C. Wang, M. Delferro and O. K. Farha, *Nat. Catal.*, 2018, **1**, 356–362.
77 R. Kalita, M. Chauhan, P. Gupta, W. Begum, C. Thadhani, B. Ghosh, Balendra, H. Bisht and K. Manna, *Chem. Commun.*, 2024, **60**, 6504–6507.
78 S. Horike, M. Dincă, K. Tamaki and J. R. Long, *J. Am. Chem. Soc.*, 2008, **130**, 5854–5855.
79 W. Zhang, G. Lu, C. Cui, Y. Liu, S. Li, W. Yan, C. Xing, Y. R. Chi, Y. Yang and F. Huo, *Adv. Mater.*, 2014, **26**, 4056–4060.
80 I. Luz, C. Rösler, K. Epp, F. X. Llabrés I Xamena and R. A. Fischer, *Eur. J. Inorg. Chem.*, 2015, **2015**, 3904–3912.
81 L. Yang, P. Cai, L. Zhang, X. Xu, A. A. Yakovenko, Q. Wang, J. Pang, S. Yuan, X. Zou, N. Huang, Z. Huang and H.-C. Zhou, *J. Am. Chem. Soc.*, 2021, **143**, 12129–12137.

82 Y. Zhao, S. Zhang, M. Wang, J. Han, H. Wang, Z. Li and X. Liu, *Dalton Trans.*, 2018, **47**, 4646–4652.
83 R. Kalita, Y. Monga and K. Manna, *New J. Chem.*, 2025, **49**, 2071–2078.
84 J. Krzystek, A. Ozarowski and J. Telser, *Coord. Chem. Rev.*, 2006, **250**, 2308–2324.
85 R. J. Holmberg, T. Burns, S. M. Greer, L. Kobera, S. A. Stoian, I. Korobkov, S. Hill, D. L. Bryce, T. K. Woo and M. Murugesu, *Chem. – Eur. J.*, 2016, **22**, 7711–7715.